Optics Communications 283 (2010) 1909–1916

Contents lists available at ScienceDirect

Optics Communications

journal homepage: www.elsevier.com/locate/optcom

Detecting characteristics of information masked by a laser-triggered microwave system via Hilbert–Huang transform

Yuo-Hsien Shiau [a,*], Ming-Chya Wu [b,c]

[a] Graduate Institute of Applied Physics, National Chengchi University, Taipei 11605, Taiwan, ROC
[b] Research Center for Adaptive Data Analysis, National Central University, Chungli 32001, Taiwan, ROC
[c] Institute of Physics, Academia Sinica, Nankang, Taipei 11529, Taiwan, ROC

ARTICLE INFO

Article history:
Received 13 July 2009
Received in revised form 15 December 2009
Accepted 15 December 2009

Keywords:
Optoelectronics
Detrended fluctuation analysis
Multiscale entropy
Empirical mode decomposition
Time series analysis

ABSTRACT

A two-wave-mixing microwave system under a delayed feedback control is proposed for chaotic communications in this study. Under the consideration of simple chaotic masking, Hilbert–Huang transform is proved to be an efficient way to detect characteristics of information signals via the spectrum of intrinsic mode functions. Based upon detrended fluctuation as well as multiscale entropy analyses on masking efficiency in the present system, we may suggest that Hilbert–Huang transform would be an alternative method to analyze complex dressed signals from nonlinear optoelectronic systems.

1. Introduction

Secure communications using chaotic waveforms has been a particular application of nonlinear dynamics appeared at the beginning of 1990s [1,2]. For example, electronic circuits modeled by nonlinear ordinary differential equations were used very often for the generation of chaotic dynamics, however, the encryption efficiency of these electronic setups is limited by the embedded low-dimensional complexity. Ikeda-type delay dynamics [3,4] has shown to be an outstanding candidate for chaos-based encryption in modern high speed optical telecommunications [5–9]. It is known that the unique feature of delay dynamics is to exhibit extremely complex chaotic behaviors, which can be quantified in terms of Lyapunov spectrum of a given chaotic regime in a reconstructed phase space of finite dimension, and finally a Lyapunov dimension is derived. Dorizzi et al. had shown that the Lyapunov dimension has linear dependence with the ratio T/τ [10], where τ is a characteristic response time and T is the delay time. Larger et al. experimentally demonstrated an Ikeda-type optoelectronics intended for practical applications, where the Lyapunov dimension can be up to 470 when T/τ equals 60 [11]. Nevertheless, as it has been shown that, for chaotic masking schemes, the hidden information can be extracted using the methods of reconstruction of time-delay systems from the time series [12,13].

Recently, it is known that fluctuations in complex systems carry important information reflecting the mechanisms underlying control processes and interactions among different components at multiple time scales. A major problem in the analysis of signals from complex systems is related to nonstationarities, e.g., mean and standard deviation vary with time. The presence of nonstationarities makes traditional approaches assuming stationary signals not reliable. To resolve the difficulties related to nonstationary behaviors, Hilbert–Huang transform (HHT), a new time–frequency representation method of signal analysis, developed by Huang et al. [14] is based on nonlinear chaotic theories and has been designed to extract dynamic information from nonstationary signals at different time scales. HHT comprises the empirical mode decomposition (EMD) and Hilbert transform. The aim of EMD is to decompose a signal into a set of intrinsic mode functions (IMFs), where the characteristics of each IMF are such that they may be Hilbert transformed. Then, through the Hilbert transform, the instantaneous frequency with meaningful feature of each IMF at any point in time may be calculated. The decomposition is based on the local time scale of the data and yields adaptive basis functions. Hence it can be used for nonlinear and nonstationary signal analysis [15]. Based upon the advantages of HHT, it would be interesting to test whether HHT could be used to extract information masked by chaotic communication systems.

To practically construct chaotic communication systems, we propose a two-wave-mixing microwave system under a delayed feedback control. These two laser beams will form a moving

* Corresponding author. Tel.: +886 2 29393091x62987; fax: +886 2 29360360.
E-mail address: yhshiau@nccu.edu.tw (Y.-H. Shiau).

0030-4018/$ - see front matter © 2009 Elsevier B.V. All rights reserved.
doi:10.1016/j.optcom.2009.12.041

interference pattern and excite electron–hole pairs in semiconductor microwave devices. According to linear stability analysis, the moving interference pattern can tunably control the emitting wavelength. When appropriate feedback parameters are considered, this nonlinear system can generate high-dimensional chaotic microwaves, therefore, could be applied to chaotic masking. Besides, in this study, both detrended fluctuation analysis (DFA) [16] and multiscale entropy (MSE) [17,18] will be used to analyze masking efficiency in our chaos-based encryption. Based upon simulation results, we might suggest that EMD would be an efficient way for multiscale separation, and finally extract characteristics of information from the nonlinear two-wave-mixing system.

The remainder of this paper is organized as follows. The two-wave-mixing system as well as associated stability analysis will be described in Section 2. Section 3 will briefly address DFA and MSE for the test of masking efficiency in our communication system. Sections 4 and 5 contain the central part of this study including extraction of information via HHT and discussions, respectively. Concluding remarks are given in Section 6.

2. Nonlinear two-wave-mixing system

Numerical/experimental studies on light-induced multiple transient gratings in semi-insulating GaAs had been performed [19,20]. One of interesting results is the spatial period of the light interference pattern and the drift velocity of multiple high-field profiles (domains) will determine the oscillating frequency of photocurrent in nanosecond duration. Therefore, tunable control of the emitting wavelength by use of the wave-mixing technique can be expected. In order to analytically explain this interesting finding, in this study we consider two optical waves are incident on a biased shallow-impurity-doped GaAs as shown in Fig. 1. Taking the light energy just above the band gap of GaAs, 10-ns duration Nd:YAG laser pulses, we can generate electron–hole pairs by optical excitation. The intensity $I(x,t)$ of the mixing waves moving through the n-GaAs is given by $I(x,t)=I_0[1+m\cos(Kx+\Omega t)]$, where Ω is the frequency difference of the two optical waves, $K=2\pi/\Lambda$ the interference wave number, Λ the grating period, m the modulation depth of the interference grating, and I_0 the average intensity. The generation–recombination processes include complete thermal ionization of donors, generation of electron–hole pairs by the optical waves at rate g, and recombination of electron–hole pairs with rate γ. The dynamical equations include the Gauss law, the continuity equations of electrons and holes, and the circuit equation

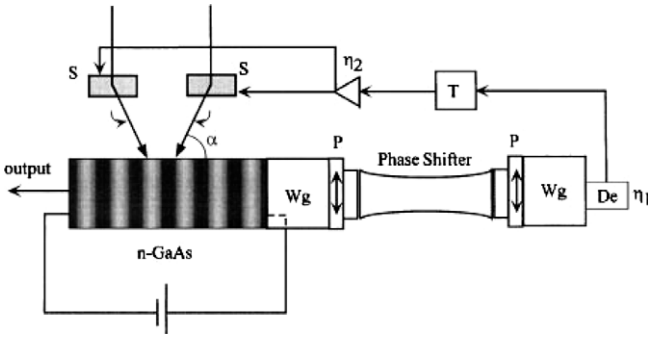

Fig. 1. The proposed experimental setup consists of a pair of waveguides *Wg*, a phase shifter whose fast and slow axes are at 45° to a pair of crossed polarizers *P*, a detector D_e with a time response $\tau\sim 10$ ns, a delay line with retardation time $T\sim 1$ μs, amplifiers η_1 and η_2, and a pair of acousto-optic scanners *S* to tune the incident angle α of the laser beams.

$$\frac{\partial E}{\partial x}=\frac{e}{\epsilon}(n-N_D^*-p), \tag{1}$$

$$\frac{\partial n}{\partial t}=gI(x,t)-\gamma np-\frac{\partial}{\partial x}\left[n\upsilon(E)-D_n\frac{\partial n}{\partial x}\right], \tag{2}$$

$$\frac{\partial p}{\partial t}=gI(x,t)-\gamma np+\frac{\partial}{\partial x}\left[p\mu_p E+D_p\frac{\partial p}{\partial x}\right], \tag{3}$$

$$V=\int_0^L E(x,t)dx, \tag{4}$$

where n, p, N_D^*, L, V, and E are, respectively, the free electron density, the free hole density, the effective donor concentration, the sample length, the applied bias, and the electric field. D_n and D_p denote, respectively, the diffusion coefficients of electron and hole; μ_p and $\upsilon(E)$ are the hole mobility and the electron drift velocity, respectively. Due to the band structure of GaAs, we know that $\upsilon(E)$ displays N-shaped negative differential mobility (NDM) [21].

We use a Fourier series to solve Eqs. (1)–(4) with complete basis functions $\{e^{il(Kx+\Omega t)}\}$, where $|l|$ is a positive integer, chosen based on the moving interference pattern of $I(x,t)$. Therefore, the solutions of Eqs. (1)–(4) be described as follows:

$$E(x,t)=E_0+\sum_{l\neq 0}\bar{m}^{|l|}E_l(t)e^{il(Kx+\Omega t)}, \tag{5}$$

$$n(x,t)=n_0+\sum_{l\neq 0}\bar{m}^{|l|}n_l(t)e^{il(Kx+\Omega t)}, \tag{6}$$

$$p(x,t)=p_0+\sum_{l\neq 0}\bar{m}^{|l|}p_l(t)e^{il(Kx+\Omega t)}, \tag{7}$$

$$\upsilon(E)=\upsilon_0+\sum_{j=1}^{\infty}\frac{\upsilon_0^{(j)}}{j!}\left[\sum_{l\neq 0}\bar{m}^{|l|}E_l(t)e^{il(Kx+\Omega t)}\right]^j, \tag{8}$$

where $\bar{m}=m/2$, $\upsilon_0=\upsilon(E_0)$ and $\upsilon_0^{(j)}=\frac{d^j\upsilon(E)}{dE^j}|_{E=E_0}$. Note that the hole density $p(x,t)$ in Eq. (7) can be expressed in terms of the electric field $E(x,t)$ and electron density $n(x,t)$ via the relation in Eq. (1). Furthermore, Eqs. (5)–(8) converge when the modulation depth m is much smaller than 1. Then we can generate the solutions of Eqs. (1)–(4) in order.

The zero-order solutions (E_0, n_0, and p_0) of Eqs. (1)–(4) are independent of space and time, thus it is straightforward to determine $E_0=V/L$, $n_0=\left(N_D^*+\sqrt{N_D^{*2}+4gI_0/\gamma}\right)/2$, and $p_0=\left(-N_D^*+\sqrt{N_D^{*2}+4gI_0/\gamma}\right)/2$. For simplicity, from now on we consider the case when the free electrons are mostly from the donor impurities and the average intensity I_0 is very small so that $n_0\approx N_D^*$. The first-order solutions (E_1, n_1, and p_1) can be obtained by substituting the expansions of Eqs. (5)–(8) into Eqs. (1)–(4):

$$\frac{dE_1}{dt}=-\left[\frac{e}{\epsilon}N_D^*\upsilon_0^{(1)}+K^2D_p+i(\Omega-KE_0\mu_p)\right]E_1 +\frac{e}{\epsilon}\left[iK(D_n-D_p)-(\upsilon_0+E_0\mu_p)\right]n_1, \tag{9}$$

$$\frac{dn_1}{dt}=gI_0-iKN_D^*\left(\upsilon_0^{(1)}-\frac{\epsilon}{e}\gamma\right)E_1 -\left[\gamma N_D^*+K^2D_n+i(\Omega+K\upsilon_0)\right]n_1. \tag{10}$$

The solutions E_1 and n_1 can be divided into $E_{1,s}+E_{1,t}$ and $n_{1,s}+n_{1,t}$, respectively. The indices s and t denote steady-state and time-dependent solutions, respectively. The steady-state solutions are

$$n_{1,s}=\Gamma\times E_{1,s}, \tag{11}$$

$$E_{1,s}=gI_0\times\Psi^{-1}, \tag{12}$$

where $\Gamma=\left[\frac{e}{\epsilon}N_D^*\upsilon_0^{(1)}+K^2D_p+i(\Omega-KE_0\mu_p)\right]/\left[\frac{e}{\epsilon}[iK(D_n-D_p)-(\upsilon_0+E_0\mu_p)]\right]$ and $\Psi=iKN_D^*\left(\upsilon_0^{(1)}-\frac{\epsilon}{e}\gamma\right)+[\gamma N_D^*+K^2D_n+i(\Omega+K\upsilon_0)]\Gamma$.

The $E_{1,t}$ and $n_{1,t}$ have time dependence $\sim e^{\bar{\Lambda}t}$, where $\bar{\Lambda} = -\gamma N_D^* - K^2 D_p + i(KE_0\mu_p - \Omega)$ or $-\frac{e}{\epsilon}N_D^* v_0^{(1)} - k^2 D_n - i(\Omega + K v_0)$, which are obtained from Eqs. (9) and (10). Hence the first-order solution for the electric field can be expressed as

$$E_1 e^{i(Kx+\Omega t)} = E_{1,s} e^{i(Kx+\Omega t)} + c_1 e^{-(\gamma N_D^* + K^2 D_p)t} e^{iK(x+E_0\mu_p t)} + c_2 e^{-\left(\frac{e}{\epsilon}N_D^* v_0^{(1)} + K^2 D_n\right)t} e^{iK(x-v_0 t)}, \quad (13)$$

where c_1 and c_2 are constants. The first term on the right hand side of Eq. (13) shows the space-charge field induced by the optical-wave mixing, which has the same phase velocity as the moving interference pattern. The second term has phase velocity $\mu_p E_0$, but vanishes as $t \to \infty$. The third term demonstrates the multiple field-domain formation when $-\left(\frac{e}{\epsilon}N_D^* v_0^{(1)} + K^2 D_n\right) > 0$ (note that $v_0^{(1)} < 0$), the domain velocity is v_0, and the distance between adjacent domains is $\Lambda = K/2\pi$. Since $n_0 \approx N_D^*$, the space-charge field can be neglected. Therefore, the underlying physics in Eq. (13) is that the external laser beams will create a periodic domain train with wave number K, but the domain train still sustains the drift velocity $v_0 (\approx 10^7$ cm/s), which is not influenced by the phase velocity Ω/K of the interference pattern. Therefore, the interference pattern will control the wavelength Λ of the microwave which is equal to $\frac{1}{2}c\Lambda_l v_0^{-1}\cos^{-1}\alpha$, where c is the speed of light and Λ_l is the wavelength of the laser beams.

Fig. 1 shows the two-wave-mixing nonlinear system can be tunably controlled in wavelength Λ. The feedback loop consists of a pair of waveguides Wg, a phase shifter whose fast and slow axes are at 45° to a pair of crossed polarizers P, a detector D_e, i.e., planar-doped barrier diode, with a time response $\tau \sim 10$ ns, a delay line with retardation time $T \sim 1$ μs, and a pair of acousto-optic scanners S to tune the incident angle α of the laser beams. The microwave radiation power P_m from n-GaAs can be expressed as $E_{rf}^2 v_0^2 R^{-1} c^{-2} \Lambda^2$ [22], where E_{rf} and R correspond to the rf field and resistance in the semiconductor, respectively. P_m is collected by a Wg and modulated by a phase shifter. The phase shifter induces the nonlinear power function $P_m \sin^2(\pi D/\Lambda)$ detected by D_e with a gain η_1, where D is the length of the phase shifter. The purpose of D_e is to convert the nonlinear power into an electric current $i(t)$. The current is then retarded by a delay line and enhanced by an amplifier with a gain η_2, then it drives S, tuning the incident angle of the laser beams. If the variation of α is linearly proportional to i with a ratio a, it is easy to get the relation between $\Lambda(t)$ and $i(t) : \Lambda(t) = \Lambda_0 + Ai(t)$, where $A \equiv a\Lambda_0 \tan\alpha_0$ and Λ_0 is the initial wavelength due to the initial incident angle α_0. Therefore, the circuit equation for this nonlinear system is

$$\tau\frac{d\Lambda(t)}{dt} + \Lambda(t) = \Lambda_0 + A\eta_1\eta_2 P_m(t-T)\sin^2\left[\frac{\pi D}{\Lambda(t-T)}\right]. \quad (14)$$

For convenience of analysis, we make Eq. (14) dimensionless

$$\frac{\tau}{T}\frac{d\Lambda_D(t_D)}{dt_D} + \Lambda_D(t_D) = 1 + \beta\Lambda_D^2(t_D - 1)\sin^2\left[\frac{\pi D}{\Lambda_0}\frac{1}{\Lambda_D(t_D-1)}\right], \quad (15)$$

where $\Lambda(t)/\Lambda_0 \to \Lambda_D(t)$, $t/T \to t_D$, and $\beta = a\Lambda_0^2\eta_1\eta_2\tan\alpha_0 E_{rf}^2 v_0^2/Rc^2$. There are two important parameters in Eq. (15), D/Λ_0 and β. The experimental process for tuning these two parameters can be understood as follows. Selecting an arbitrary α_0 to create initial wavelength Λ_0, then D/Λ_0 is determined by α_0, since D is fixed. When t is larger than T, the feedback loop begins to work. We only need to tune the gain of amplifier to effectively change the β value in Eq. (15). Therefore, D/Λ_0 and β in Eq. (15) correspond to α_0 and η_2 in the experiment, respectively.

3. Statistical tests for masking efficiency

We first generate a periodic square-wave train as the original signal $o(t)$ shown in Fig. 2(a), where the oscillating period is equal to 400 (dimensionless). This time series is considered to carry a meaningful information. To dress the square wave for secure communications, a coding signal $n(t)$ (i.e., $\Lambda_D(t)$) generated by Eq. (15), where $D/\Lambda_0 = 1.4$, $\beta = 0.725$, and $T/\tau = 100$ are considered, is then added to the square wave to become an encoded signal [23]. The coding signal is shown in Fig. 2(b), and the encoded signal $e(t)$ is shown in Fig. 2(c). The relation between $o(t)$, $n(t)$ and $e(t)$ is

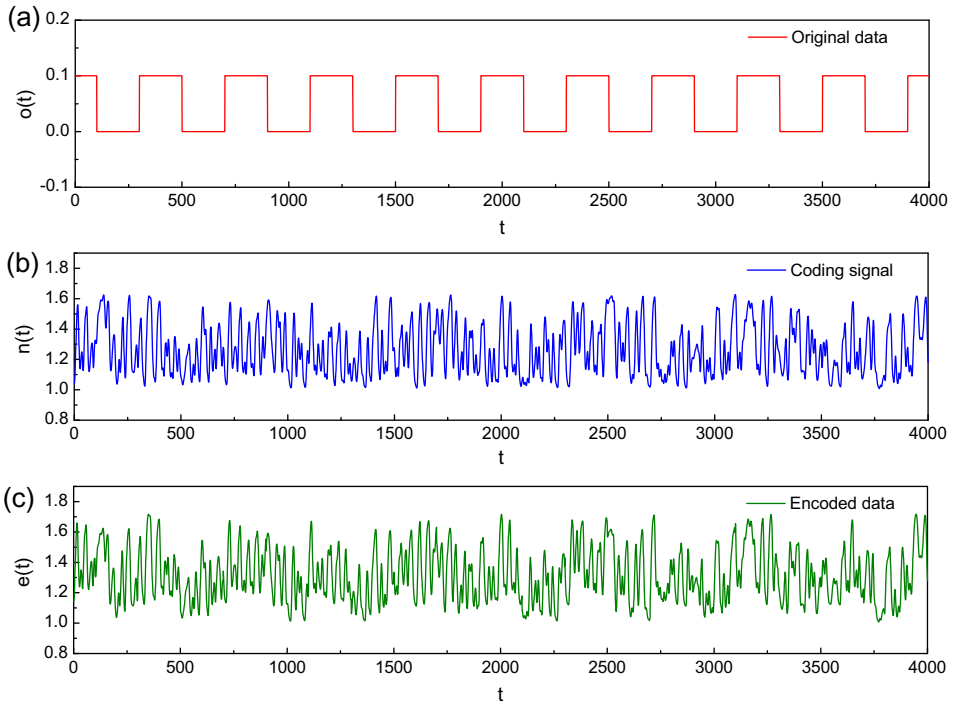

Fig. 2. (a) Original signal $o(t)$, (b) coding signal $n(t)$, and (c) encoded signal $e(t)$, where all variables are dimensionless.

$$e(t) = o(t) + n(t). \tag{16}$$

In this study, we use different ways to test masking efficiency, of which the characteristics of $e(t)$ should not have significant differences with respect to that of the time series $n(t)$. These conditions guarantee the encoding is suitable for secure communications. To ensure the coding is good enough, applying DFA [16] as well as MSE [17,18] on $n(t)$ and $e(t)$ give similar statistical characteristics (Fig. 3). For DFA, the relation between fluctuation $F(l)$ and sampling length l in log–log scale is shown in Fig. 3(a), in which the slope measured at large l regime is usually unreliable for a limited data length. Therefore, the slight deviation between two plots around $\log_{10} l = 2.5$ does not suggest a significant difference between these two time series. As for MSE, Fig. 3(b) shows similar profiles of the measure $H(l)$ in different scale for the coding signal $n(t)$ and encoded signal $e(t)$ [24]. Thus the effectiveness of the encoding is then examined. Detailed descriptions about DFA and MSE are shown in Appendix.

4. Hilbert–Huang transform

The aim of the EMD is to decompose the signal into a sum of IMFs. An IMF represents a simple oscillatory mode as a counterpart

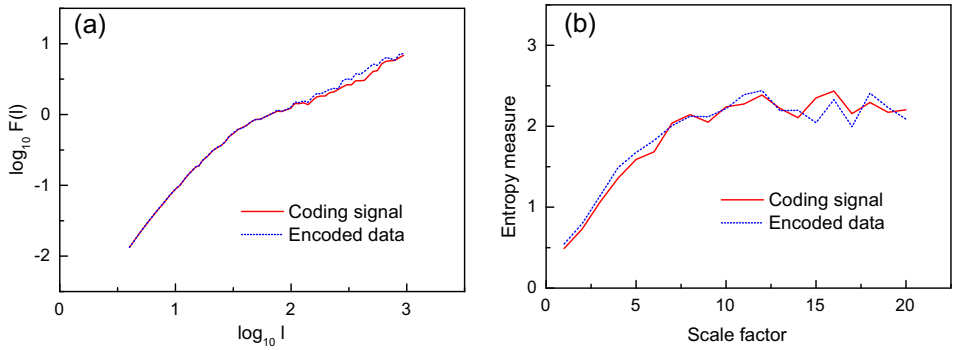

Fig. 3. (a) DFA analysis and (b) multiscale entropy measure for the coding signal and encoded signal.

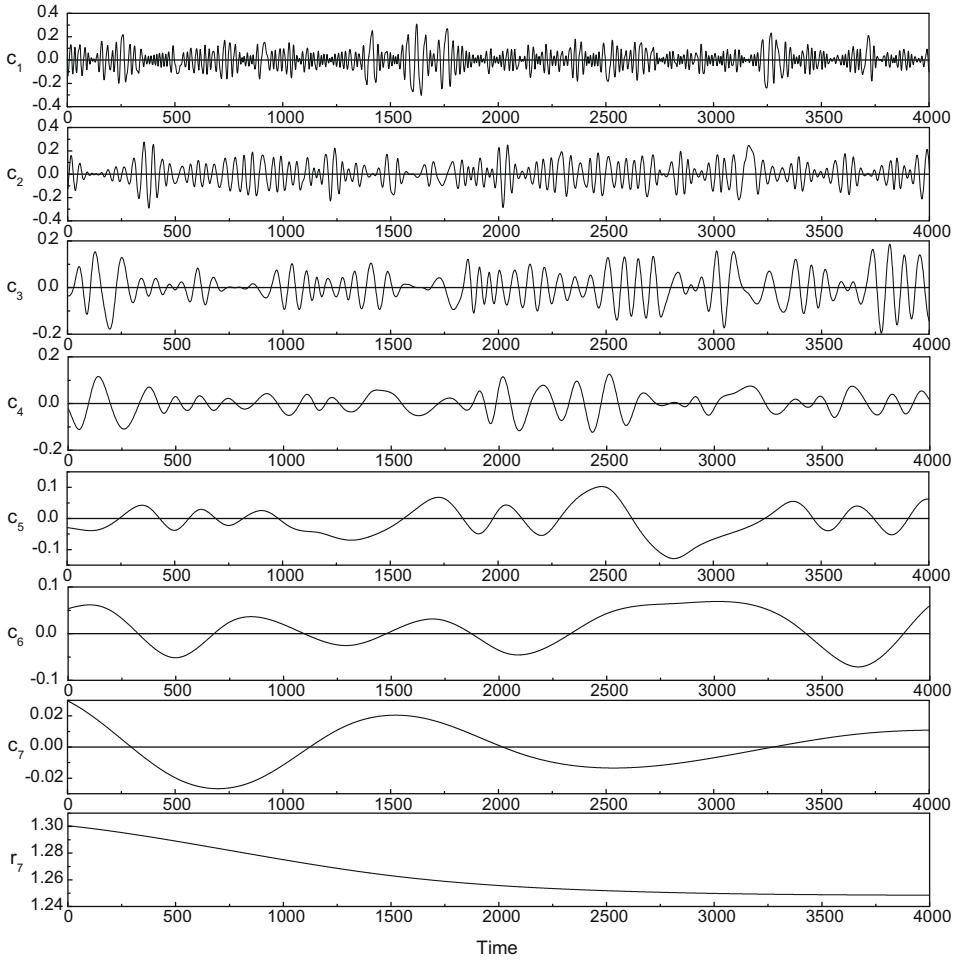

Fig. 4. EMD for the coding signal $n(t)$. The time series is decomposed into seven IMFs $(c_1, \ldots, c_7)$ and a residue r_7.

to the simple harmonic function used in Fourier analysis. The implementation is carried by sifting data to generate IMFs. The IMFs introduced by the EMD are a set of well-behaved intrinsic modes, and are symmetric with respect to the local mean and have the same numbers of zero crossings and extremes. The resultant IMFs obtained by EMD form a complete set, in which these IMFs are orthogonal to each other. To create IMFs, the first thing is to identify the local extremes in the data $\{x(t)\}$. Then, all the local maxima are connected by a cubic spline line $U(t)$ while the same procedure is applied for the local minima to produce the lower envelope $L(t)$. Both envelopes will cover all of the original data. The mean of upper envelope and the lower envelope, $m_1(t)$, given by

$$m_1(t) = \frac{U(t) + L(t)}{2} \tag{17}$$

is a running mean. Subtracting the running mean $m_1(t)$ from the original data $x(t)$, we get the first component $h_1(t)$,

$$h_1(t) = x(t) - m_1(t). \tag{18}$$

The resulting component $h_1(t)$ is an IMF if it satisfies the following conditions: (i) $h_1(t)$ is free of riding waves. (ii) It displays symmetry of the upper and the lower envelopes with respect to zero. (iii) The number of zero crossings and extremes are the same, or only differ by 1. If $h_1(t)$ is not an IMF, the sifting process has to be repeated as many times as is required to reduce the extracted signal to an IMF. In the subsequent sifting process steps, $h_1(t)$ is treated as the datum to repeat steps mentioned above,

$$h_{11}(t) = h_1(t) - m_{11}(t). \tag{19}$$

Again, if the function $h_{11}(t)$ does not yet satisfy criteria (i)–(iii), the sifting process continues up to k times until some acceptable tolerance is reached:

$$h_{1k}(t) = h_{1(k-1)}(t) - m_{1k}(t). \tag{20}$$

If the resulting time series is the first IMF, it is designated as $c_1 = h_{1k}(t)$. The first IMF is then subtracted from the original data, and the difference r_1 given by

$$r_1(t) = x(t) - c_1(t), \tag{21}$$

is the first residue. The residue $r_1(t)$ is taken as if it were the original data and is applied again the sifting process stated above.

Following the above procedures, one continues the process to find more intrinsic modes c_i until the last one. The final residue will be a constant or a monotonic function that represents the general trend of the time series [14,15]. Finally, we have

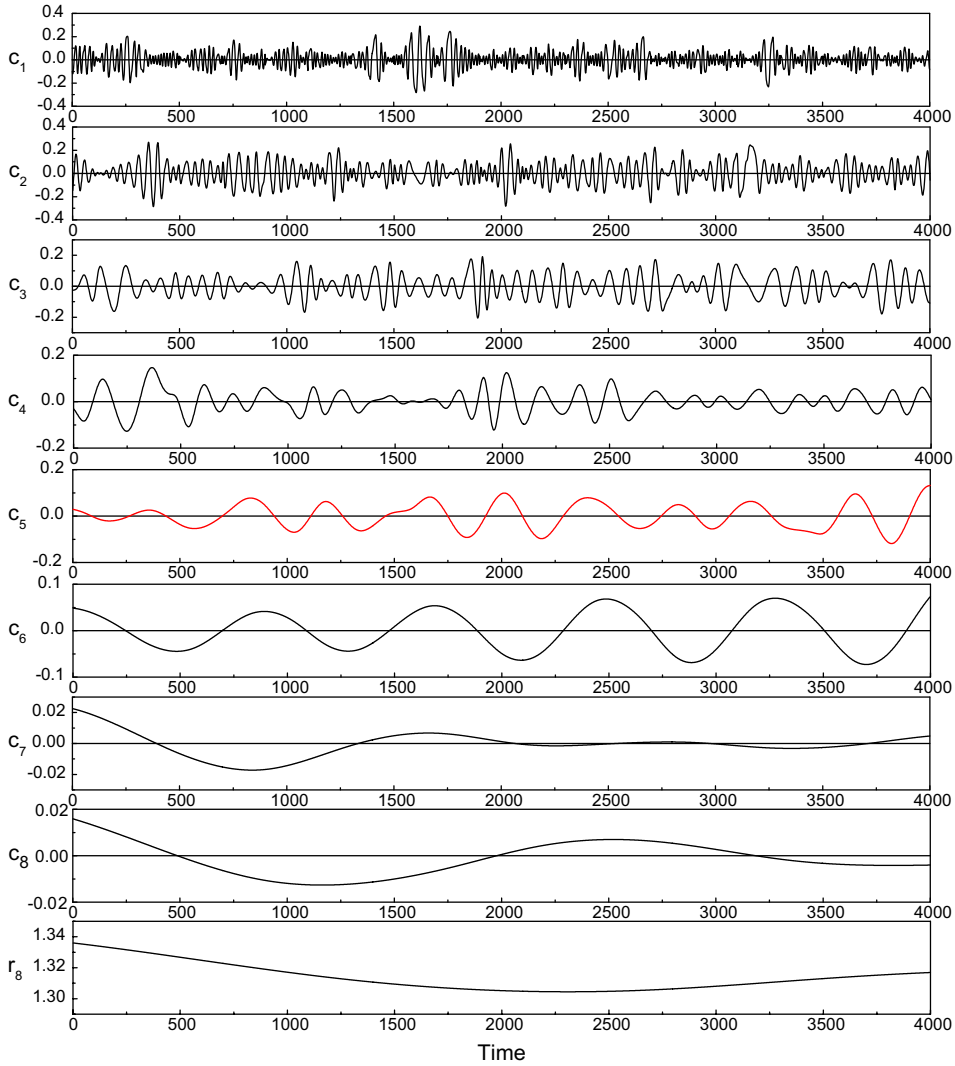

Fig. 5. EMD for the encoded signal $e(t)$. The time series is decomposed into eight IMFs ($c_1, \ldots, c_8$) and a residue r_8. In particular, IMF c_5 is depicted in red. (For interpretation of the references to colour in this figure legend, the reader is referred to the web version of this article.)

$$x(t) = \sum_{i=1}^{n} c_i(t) + r_n(t), \tag{22}$$

$$r_i(t) = r_{i-1}(t) - c_i(t). \tag{23}$$

The decompositions of $n(t)$ and $e(t)$ are shown in Figs. 4 and 5. The time series of $n(t)$ is decomposed into seven IMFs and a residue, while $e(t)$ is decomposed into eight IMFs and a residue. Comparing two decompositions, it is apparent that the decomposition of $e(t)$ has an extra mode in its c_5 IMF. Moreover, it is reasonable to eliminate the trend obtained in the EMD. We then normalize the amplitude of IMFs according to the following rules:

$$nc_i = \frac{c_i}{r_n}. \tag{24}$$

The normalized IMFs nc_i for the coding signal $n(t)$ and encoded signal $e(t)$ are shown in Fig. 6.

The Hilbert transform can now be applied on nc_i. For the kth mode, this can be done by first calculating the conjugate pair of $nc_k(t)$, i.e.,

$$z_k(t) = \frac{1}{\pi} P \int_{-\infty}^{\infty} \frac{nc_k(t')}{t - t'} dt', \tag{25}$$

where P indicates the Cauchy principal value. With this definition, the two functions $nc_k(t)$ and $z_k(t)$ forming a complex conjugate pair define an analytic signal, and we have

$$nc_k(t) + iz_k(t) = A_k(t) e^{i\phi_k(t)} \tag{26}$$

with the amplitude $A_k(t)$ and the phase $\phi_k(t)$ defined by

$$A_k(t) = \left[nc_k^2(t) + z_k^2(t)\right]^{1/2}, \tag{27}$$

$$\phi_k(t) = \tan^{-1}\left(\frac{z_k(t)}{nc_k(t)}\right). \tag{28}$$

In practice, we calculate the instantaneous phase according to Eqs. (25) and (28). To plot Hilbert spectra, the frequency is defined as the time derivative of phase in Eq. (28). The Hilbert spectra for the normalized IMFs of $n(t)$ and $e(t)$ are shown in Fig. 7. The power spectral density (PSD) as a function of frequency for $n(t)$ and $e(t)$, calculated from the Hilbert spectra of the normalized IMFs of $n(t)$ and $e(t)$ (Fig. 7), is shown in Fig. 8. Note that there is a peak at 0.0025 (dimensionless) corresponding to the IMF c_5 in the decomposition of $e(t)$. The appearance of the peak may be considered as a signature of the buried signal. Fig. 9 shows the comparison of $o(t)$, IMF c_5 and normalized IMF nc_5 of $e(t)$. Except for the boundary effect, both c_5 and nc_5 exhibit the similar oscillating characteristics as $o(t)$. Hence, the decomposition of $e(t)$ to IMFs has successfully captured the specific feature of the buried signal $o(t)$. As for the problem of distorted waveforms appeared both in c_5 and nc_5, to our knowledge the EMD method can not guarantee to recover the original waveform. However, the variance of c_5 is very close to that of $o(t)$ rather than those of other decomposed IMFs, where the variance deviation between c_5 and $o(t)$ is roughly equal to 15%. Thus, based upon results shown in above we may conclude that

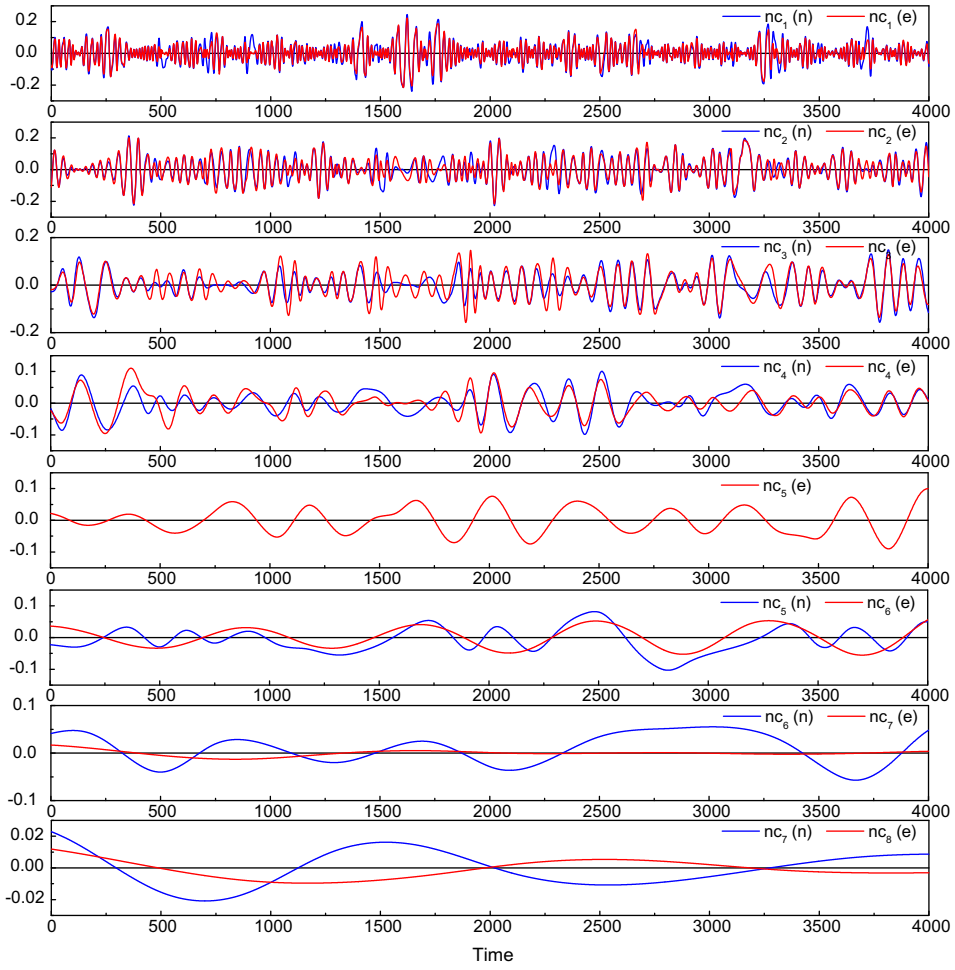

Fig. 6. Normalized IMFs of $n(t)$ (blue line) and $e(t)$ (red line). (For interpretation of the references to colour in this figure legend, the reader is referred to the web version of this article.)

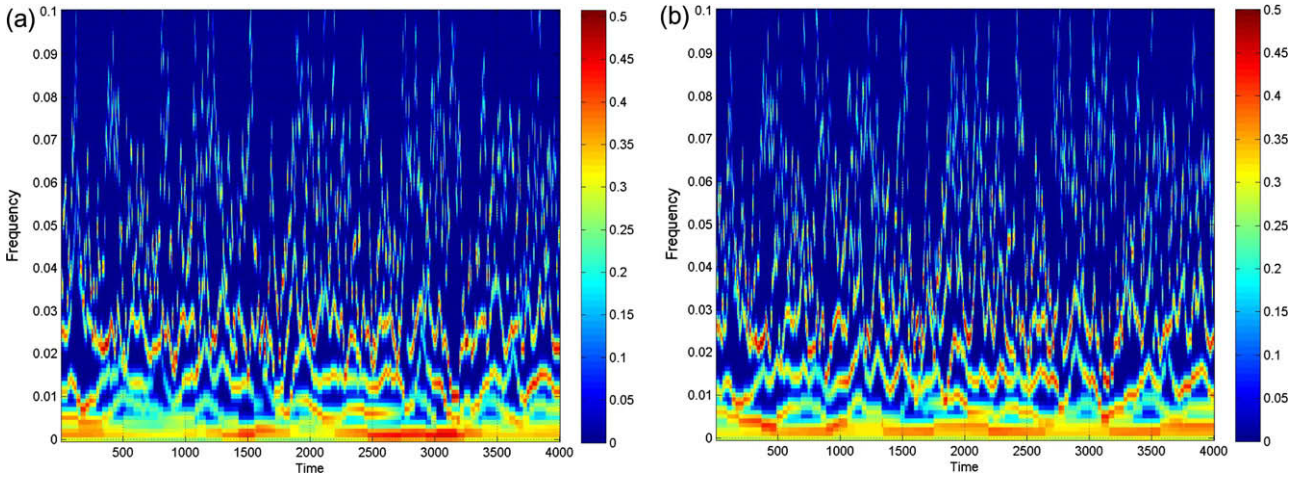

Fig. 7. Hilbert spectra for the normalized IMFs of (a) $n(t)$ and (b) $e(t)$.

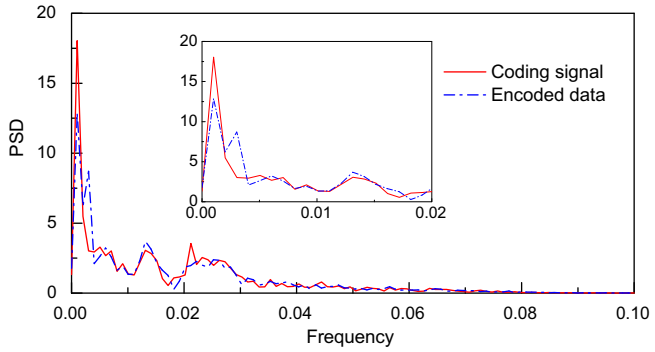

Fig. 8. Power spectral density (PSD), calculated from the Hilbert spectra shown in Fig. 7, for $n(t)$ and $e(t)$. In order to clearly visualize the peak located at 0.0025, the enlarged diagram is shown in the inset.

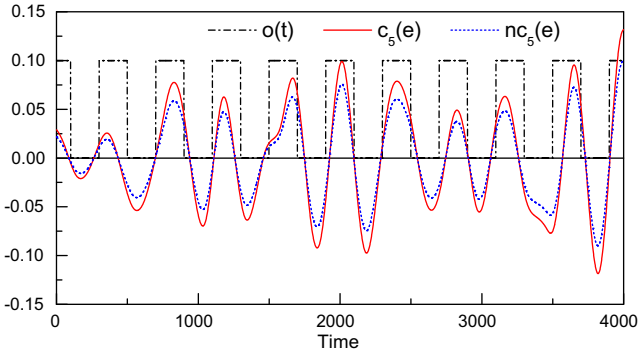

Fig. 9. Illustrations of $o(t)$, IMF c_5 and normalized IMF nc_5 of $e(t)$.

EMD is an efficient way to detect characteristics of the information signal masked by the present two-wave-mixing microwave system with high complexity.

5. Discussions

It is known that investigations on illuminated transport in semiconductors are very important for optoelectronics [25]. In this study, tunable periodic domains can be established by use of the two-wave-mixing technique, where the difference between the high-to-low electric fields can be up to 100 kV/cm. Based upon the Pockels effect (i.e., the linear electro-optic effect) [26], a change in the refractive index is expected. And these alternating values for the refractive index modulation produce a phase grating whose diffraction pattern can be calculated/observed. Compared to the similar study in semi-insulating semiconductors [27], our system can generate a large change in the refractive index, hence which would be useful in the development of optoelectronics. However, in practical situations the period of oscillating photocurrent should be smaller than the time duration of a laser pulse, i.e., 10 ns. Therefore, the following inequality should be satisfied:

$$\frac{\Lambda}{v_0} \leqslant 10\ \text{ns}. \tag{29}$$

According to this inequality, we can estimate L and Λ should be, respectively, larger and smaller than 0.1 cm.

It should be noted that delay-induced bistability also can be found in this optoelectronic device. In order to analytically understand this phenomena, the following extreme case is introduced. If we consider τ/T tends to zero and take the adiabatic approximation, Eq. (15) will become a nonlinear difference equation

$$\Lambda_D(t_D) = 1 + \beta\Lambda_D^2(t_D - 1)\sin^2\left[\frac{\pi D}{\Lambda_0}\frac{1}{\Lambda_D(t_D - 1)}\right]. \tag{30}$$

Therefore, the steady-state solutions can be easily derived via Eq. (30) as well as $\Lambda_D(t_D) = \Lambda_D(t_D - 1)$, and multiple roots are possible to exist. Compared to the well-known optical bistability [3,4], our optoelectronic device provides an alternative way to investigate bistable phenomena.

Concerning the possible usefulness of EMD applied to chaotic communications, it shall be noted that there are some limitations in real situations. In extracting the message they have linked the message to a particular IMF for the encoded signal because this has no analog IMF for the original signal alone. However, in many signal transmission processes the original signal will not be sent, therefore, it would be impossible to extract message by use of directly comparing IMFs. In addition, the IMF analysis technique needs prior knowledge of the hidden information, which will reduce the possible applications in secure communications. The present study is not intended to develop a breaking method for chaotic communications, but provides an alternative method to analyze complex dressed signals.

6. Conclusion

We have introduced an EMD scheme to extract information masked by a two-wave-mixing microwave system, in which both DFA and MSE are used to test the statistical difference in between the coding signal $n(t)$ and the encoded signal $e(t)$. According to decomposed IMFs, temporal as well as statistical characteristics of the buried signal can be extracted. Therefore, our study suggests that HHT would be an alternative method to analyze complex dressed signals from nonlinear optoelectronic systems.

Acknowledgements

This work was supported by the National Science Council of the Republic of China (Taiwan) under Grant Nos. NSC 95-2119-M-002-001 (M.-C. Wu), and NSC 95-2112-M-259-010-MY3 (Y.-H. Shiau).

Appendix

DFA approach

The method is described briefly in the following. The time series $x(i)$ to be analyzed is first integrated and denoted as $y(i)$, where $i = 1, \ldots, N$ and N is the length of the series. Next, the integrated time series is divided into boxes of equal length, l. In each box of length l, a least squares line (or polynomial curves) is fitted to the data to represent the trend in that box. Next, the integrated time series is detrended by subtracting the local trend in each box. The root-mean-square fluctuation of this integrated and detrended time series is calculated and denoted as the 1st order fluctuation function $F(l)$. This computation is repeated over all box sizes to characterize the relationship between $F(l)$ and l. Typically, $F(l)$ will increase with the box size l. A linear relationship in a log–log plot indicates the presence of a monofractal spectrum:

$$F(l) \propto l^{\gamma} \tag{31}$$

In general, it is not always to exhibit a power-law scaling for analyzed data. On the contrary, exponent γ could be different in different box size l. It would be helpful to understand the statistical meaning of the exponent γ through the following explanations. For stationary data with scale-invariant temporal organization, the Fourier power spectrum is proportional to $f^{-\beta}$, where the scaling exponent β is related to γ with that way, $\beta = 2\gamma - 1$. Thus time series with the $1/f$ characteristic (i.e., $\beta = 1$), sometimes named positive correlations, is characterized by exponent γ being equal to 1. As for Gaussian white noise of the flat band, $\beta = 0$ and, therefore, $\gamma = 0.5$. When β is smaller than 0, i.e., $\gamma \leqslant 0.5$, it indicates negative correlations are predominant in the original data.

MSE approach

The MSE analysis is to measure the entropy of a signal $x(t)$ in different scale. Briefly, this analysis constructs consecutive coarse-grained time series by averaging a successively increasing number of data points in nonoverlapping windows. For scale 1, the coarse-grained time series is the original time series. For scale 2, the time series is made up of the average of consecutive pairs of data points, so that its length is the length of the original time series divided by the scale factor l, and so on. Then, entropy H is calculated for each of the coarse-grained time series in the following:

$$H(l) = -\sum_{y_l(t)} \Pr(y_l(t)) \log [\Pr(y_l(t))], \tag{32}$$

$$y_l(t) = \frac{1}{l} \sum_{j=0}^{l-1} x(t+j), \quad 1 \leqslant j \leqslant L/l. \tag{33}$$

where $\Pr(y_l(t))$ denotes the probability of the value $y_l(t)$.

References

[1] L.M. Pecora, T.L. Carroll, Phys. Rev. Lett. 64 (1990) 821.
[2] K.M. Cuomo, A.V. Oppenheim, Phys. Rev. Lett. 71 (1993) 65.
[3] K. Ikeda, Opt. Commun. 30 (1979) 257.
[4] H.M. Gibbs, F.A. Hopf, D.L. Kaplan, R.L. Schoemacker, Phys. Rev. Lett. 46 (1981) 474.
[5] G.D. VanWiggeren, R. Roy, Science 279 (1998) 1198.
[6] J.P. Goedgebuer, L. Larger, H. Porte, Phys. Rev. Lett. 80 (1998) 2249.
[7] A. Uchida, S. Yoshimori, M. Shinozuka, T. Ogawa, F. Kannari, Opt. Lett. 26 (2001) 866.
[8] S. Tang, J.M. Liu, Opt. Lett. 26 (2001) 1843.
[9] V.S. Udaltsov, J.P. Goedgebuer, L. Larger, W.T. Rhodes, Opt. Commun. 195 (2001) 187.
[10] B. Dorizzi, B. Grammaticos, M. Le Berre, Y. Pomeau, E. Ressayres, A. Tallet, Phys. Rev. A 35 (1987) 328.
[11] L. Larger, J.P. Goedgebuer, V. Udaltsov, C.R. Phys. 5 (2004) 669.
[12] M.J. Bunner, M. Popp, Th. Meyer, A. Kittel, J. Parisi, Phys. Rev. E 54 (1996) 3082.
[13] R. Hegger, M.J. Bunner, H. Kantz, A. Giaquinta, Phys. Rev. Lett. 81 (1998) 558.
[14] N.E. Huang, Z. Shen, S.R. Long, M.C. Wu, H.H. Shih, Q. Zheng, N.C. Yen, C.C. Tung, H.H. Liu, Proc. R. Soc. Lond. A 454 (1998) 903.
[15] N.E. Huang, S.S.P. Shen, Hilbert–Huang Transform and its Applications, World Scientific, Singapore, 2005.
[16] C.K. Peng, S. Havlin, H.E. Stanley, A.L. Goldberger, Chaos 5 (1995) 82.
[17] M. Costa, A.L. Goldberger, C.K. Peng, Phys. Rev. Lett. 89 (2002) 068102.
[18] M. Gosta, A.L. Goldberger, C.K. Peng, Phys. Rev. Lett. 95 (2005) 198102.
[19] L. Subačius, V. Gružinskis, P. Shiktorov, E. Starikov, K. Jarašiünas, L. Reggiani, Opt. Lett. 24 (1999) 551.
[20] I. Kašalynas, L. Subačius, Appl. Phys. Lett. 89 (2006) 152104.
[21] M.P. Shaw, V.V. Mitin, E. Schöll, H.L. Grubin, The Physics of Instabilities in Solid State Electron Devices, Plenum, New York, 1992.
[22] S.M. Sze, Physics of Semiconductor Devices, Wiley, New York, 1969.
[23] The dimension of the coding signal shown in Fig. 2(b) is estimated to be 83, thus a single sharp peak can be reasonably expected in the autocorrelation function [9].
[24] The measurement involves two three parameters, namely, N, the length of the time series; m, the length of a vector constructed from the time series, and r, the Euclidean distance between two vectors. See Ref. [17] for details. Here we have used $N = 4000$, $m = 2$, and $r = 0.15$.
[25] P. Yeh, Introduction to Photorefractive Nonlinear Optics, John Wiley and Sons Inc., New York, 1993.
[26] The refractive index modulation $\delta\bar{n}$ can be expressed as $-\bar{n}^3\gamma_{41}E(x,t)$, where $\bar{n}$ is the refractive index of a pure material and γ_{41} is the electro-optic coefficient. When the wavelength of the incident light Λ is 1 μm, $\bar{n} = 3.3$ and $\gamma_{41} = 1.43 \times 10^{-10}$ cm/V for GaAs.
[27] M. Sudžius, A. Bastys, K. Jarašiunas, Opt. Commun. 170 (1999) 149.